



**HAL**  
open science

## Cr:YAG chirped pulse oscillator

Evgeni Sorokin, Vladimir Kalashnikov, Julien Mandon, Guy Guelachvili,  
Nathalie Picqué, Irina T. Sorokina

► **To cite this version:**

Evgeni Sorokin, Vladimir Kalashnikov, Julien Mandon, Guy Guelachvili, Nathalie Picqué, et al..  
Cr:YAG chirped pulse oscillator. *New Journal of Physics*, 2008, 10, 083022 (13pp). 10.1088/1367-  
2630/10/8/083022 . hal-00311427

**HAL Id: hal-00311427**

**<https://hal.science/hal-00311427>**

Submitted on 18 Aug 2008

**HAL** is a multi-disciplinary open access archive for the deposit and dissemination of scientific research documents, whether they are published or not. The documents may come from teaching and research institutions in France or abroad, or from public or private research centers.

L'archive ouverte pluridisciplinaire **HAL**, est destinée au dépôt et à la diffusion de documents scientifiques de niveau recherche, publiés ou non, émanant des établissements d'enseignement et de recherche français ou étrangers, des laboratoires publics ou privés.

## Cr<sup>4+</sup> : YAG chirped-pulse oscillator

Evgeni Sorokin<sup>1,4</sup>, Vladimir L Kalashnikov<sup>1</sup>, Julien Mandon<sup>2</sup>,  
Guy Guelachvili<sup>2</sup>, Nathalie Picqué<sup>2</sup> and Irina T Sorokina<sup>3</sup>

<sup>1</sup> Institut für Photonik, TU Wien, Gusshausstr. 27/387, A-1040 Vienna, Austria

<sup>2</sup> Laboratoire de Photophysique Moléculaire, CNRS, Université Paris-Sud,  
Bâtiment 350, 91405 Orsay Cedex, France

<sup>3</sup> Department of Physics, Norwegian University of Science and Technology,  
N-7491 Trondheim, Norway

E-mail: [evgeni.sorokin@tuwien.ac.at](mailto:evgeni.sorokin@tuwien.ac.at)

*New Journal of Physics* **10** (2008) 083022 (13pp)

Received 20 May 2008

Published 15 August 2008

Online at <http://www.njp.org/>

doi:10.1088/1367-2630/10/8/083022

**Abstract.** We demonstrate chirped-pulse operation of a Cr:YAG passively mode-locked laser. Different operation regimes of the laser are extensively investigated in the vicinity of zero dispersion both experimentally and numerically. It is shown that for a given laser configuration, transition to the positive dispersion regime allows a 5-fold increase in the output pulse energy, which is otherwise limited by the onset of the multipulsing or ‘chaotic’ mode-locking. The output pulses have 1.4 ps duration and are compressible down to 120 fs in a 3 m piece of silica fiber, enabling supercontinuum generation in a nonlinear fiber. The spectrum shape and operation stability of the chirped-pulse regime depend strongly on the amount and shape of the intracavity dispersion. The numerical model predicts the existence of the minimum amount of the positive dispersion, above which the chirped-pulse regime can be realized. Once located, the chirped-pulse regime can be reliably reproduced and is sufficiently stable for applications.

<sup>4</sup> Author to whom any correspondence should be addressed.

**Contents**

<b>1. Introduction</b>	<b>2</b>
<b>2. Experimental realization of the Cr : YAG CPO</b>	<b>3</b>
<b>3. Numerical modeling</b>	<b>6</b>
3.1. CPO modeling . . . . .	6
<b>4. Results and discussion</b>	<b>7</b>
4.1. PDR and spectrum asymmetry . . . . .	7
4.2. Effects of the GDD spectral shape: solitonic regime . . . . .	9
4.3. Scenario of the pulse destabilization . . . . .	10
<b>5. Conclusion</b>	<b>11</b>
<b>Acknowledgments</b>	<b>13</b>
<b>References</b>	<b>13</b>

**1. Introduction**

Oscillators providing stable sub-100 fs pulses in the near-infrared region around  $1.5 \mu\text{m}$  are of interest for a number of applications including infrared continuum generation [1, 2] and high-sensitivity gas spectroscopy [3]. High-output power of such oscillators is desired because it enhances the nonlinear frequency conversion and spectral broadening in the supercontinuum generation. Currently, most of the realizations of such sources are based on femtosecond Er : fiber oscillators with amplifier stages.

A solid-state implementation of such a source could be a  $\text{Cr}^{4+}$  : YAG mode-locked oscillator. In contrast to an Er : fiber oscillator, its advantages are: (i) extremely broad gain band allowing few-optical-cycle pulses, and (ii) operability in a directly diode-pumped regime [4]. One of the features of the Cr : YAG as a laser material is its relatively low useful gain, making it necessary to operate with long crystals and low-output couplers (0.2–1%), resulting in high intracavity average power, typically some tens of watts, and a very strong nonlinear interaction inside the long crystal. This promotes numerous instabilities, primarily a tendency to multipulsing [5, 6], but also results in spectral extra-broadening [7] and self-frequency shift [8].

In the negative-dispersion regime (NDR), which is typical for femtosecond oscillators, the instabilities can be suppressed by reducing the pulse energy (e.g. by increasing the repetition rate; so far, the Cr : YAG laser operation has been demonstrated at repetition rates from 65 MHz to 4 GHz [5, 9]), or by a sufficient amount of the negative group-delay dispersion (GDD). However, the latter approach results in longer pulses and narrower spectra. Since the pulse in the NDR is chirp-free, it is incompressible (at least, linearly).

To stabilize the high-energy pulse without irreversible spectral narrowing, one can operate an oscillator in the positive-dispersion regime (PDR) [10, 11]. In the PDR regime the pulse is stretched, i.e. it has picosecond width. As a result, the peak power is reduced below the instability threshold. Simultaneously, the pulse is heavily chirped (chirped-pulse oscillator, CPO [12, 13]) and its spectrum is sufficiently wide in order to allow pulse compression down to sub-100 fs width. To date, such a regime has been successfully realized in the Ti : sapphire CPOs [10], [14]–[16], which have matured to a commercially available technology. The advantage of the Cr : YAG CPO over the fiber-based CPO [17] is a comparatively low amount of the positive GDD required for the regime stabilization. Since in the fiber oscillator the pulse

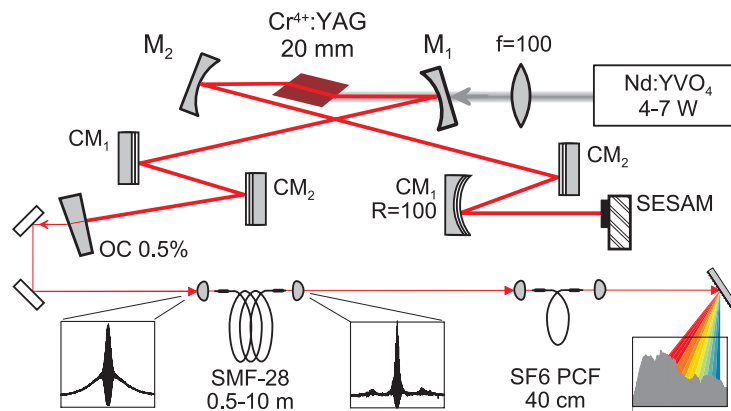


**Figure 1.** Schematic diagram of the Cr:YAG chirped-pulse oscillator. CM: chirped mirrors; OC: output coupler.

has a larger nonlinear phase shift, such a shift can be compensated only by a sufficiently large amount of the positive GDD. Around  $1.5 \mu\text{m}$  wavelength, this would have required the use of long pieces of dispersion shifted or photonic crystal fibers.

In this work, for the first time to our knowledge, we demonstrate the  $\text{Cr}^{4+}$  CPO generating picosecond chirped pulses at 100 mW average power and 140 MHz repetition rate. The pulses are compressible down to  $\approx 100$  fs and can be used for efficient supercontinuum generation in the photonic-crystal fiber (PCF). Simulations based on the generalized complex nonlinear cubic–quintic Ginzburg–Landau model present a comprehensive study of the influence of spectral dissipation as well as spectrally dependent GDD on the oscillator characteristics in both positive- and negative-dispersion regimes.

## 2. Experimental realization of the Cr:YAG CPO

The laser has been built according to the classical X-folded scheme (figure 1) on the basis of a 20 mm Cr:YAG crystal with a prismless dispersion compensation. The dichroic folding mirrors  $M_1$  and  $M_2$  had 100 mm radii of curvature and were not chirped. The scheme was close to the setup published previously [4, 18], which was shown to have been operated in Kerr-lens mode-locked configuration and with a semiconductor saturable absorber mirror (SESAM) as the starting mechanism. For dispersion compensation we used three sets of chirped mirrors, providing dispersion compensation of the YAG crystal up to the third order [4]. The three sets were designed to compensate about 5 mm of YAG crystal on a single bounce, but had GDD values differing by 25–50  $\text{fs}^2$  between 1.5 and  $1.55 \mu\text{m}$  (figure 2(a)). This allowed the dispersion to be adjusted by steps of 50–100  $\text{fs}^2$  by exchanging the mirrors. It should be noted, however, that the real dispersion of the 51-layer chirped mirrors can vary by as far as  $\pm 30 \text{fs}^2$  from the design value. Additionally, the commercial SESAM (model BATOP-SAM-1550-1) provided quite a significant amount of dispersion (figure 2(a)). Figure 2(b) shows the net dispersion with the error region which is due to the GDD uncertainty of the chirped mirrors. Since the predicted net dispersion of the setup in figure 1 is very close to zero in the 1.5– $1.55 \mu\text{m}$  region, its sign is *a priori* not known and should be defined in the experiment. Once the operating point is established, the operation regime can be reliably switched between positive and negative by

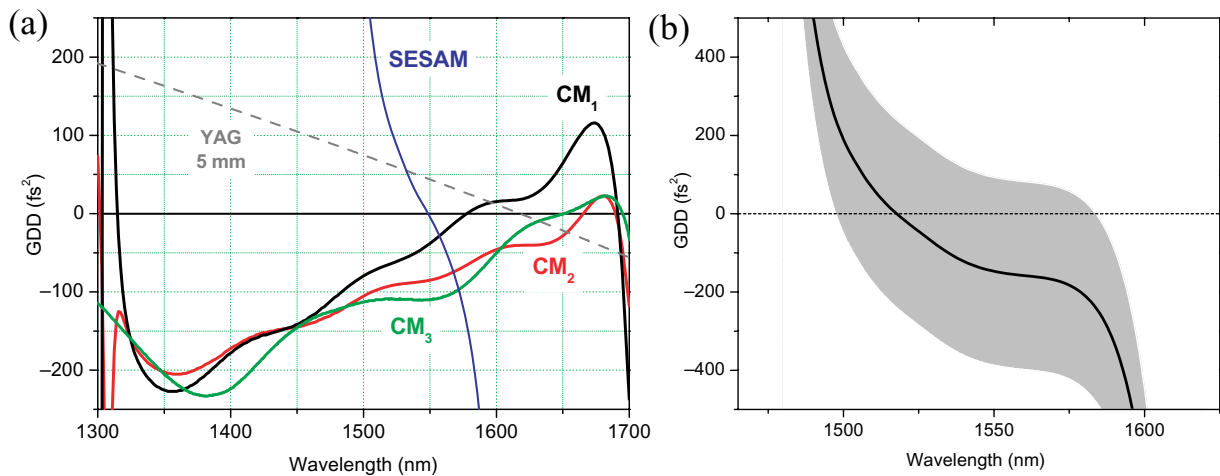


**Figure 2.** (a) GDD of three sets of chirped mirrors (as designed), the YAG crystal, and the SESAM. (b) The net dispersion of the resonator, corresponding to figure 1. Black line: as designed, gray area—uncertainty region due to the chirped mirrors.

changing the chirped mirrors or by introducing more reflections. Even simple exchange of the SESAM with the one made by a hybrid technology [4, 18] with GDD close to zero allowed the mode of operation to be switched from the positive to the negative regime. To make sure that the laser indeed operates in the positive dispersion regime, we have recorded the spectrum and the autocorrelation signal of the output radiation. Additionally, a fast photodiode was used to check if the laser is operating in a single- or multiple-pulse mode (harmonic mode-locking).

In the negative dispersion regime (e.g. with all four chirped mirrors of type CM<sub>3</sub>), the laser demonstrated a strong tendency for harmonic mode-locking, with up to 6 pulses per round-trip time. The 85 fs clean, nearly sech<sup>2</sup>-shaped pulses were equally spaced within the 7 ns time window, resulting in a pulse repetition rate of up to 867 MHz, but pulse energy of only  $\approx 100$  pJ. When the cavity was optimized for single-pulse operation by adjusting the positions of the crystal, the SESAM and the focusing mirrors, the laser switched to a ‘chaotic’ mode-locking regime [19], with unstable noisy spectrum and average output power of 200 mW. The pulse duration could not be measured because of the instability of the autocorrelation signal. The highest output pulse energy that could be obtained in the stable single-pulse regime was about 200 pJ (30 mW average power).

With different chirped mirrors, corresponding to less negative GDD as in figure 2(b), the laser behavior dramatically changed. Firstly, the laser operation became stable and single-pulsed with a repetition rate of 144.5 MHz and an output power of up to 150 mW, corresponding to 1 nJ pulse energy. Secondly, the output spectrum has acquired a characteristic shape (figure 3) with sharply cut edges at both sides. The strongly nonexponential character of the spectral edges is especially vivid on the logarithmic scale (figure 3(b)). Finally, the pulses have acquired a significant chirp as shown in figure 4. The spectrum shape and the chirp resemble the typical features of the positive-dispersion regime in Ti : sapphire oscillators [10], [12]–[16].

Since the sign of the net intracavity dispersion cannot be unambiguously defined due to the uncertainties in the dispersion of the chirped mirrors, we need additional evidence that the laser indeed operates in the positive dispersion regime. This can be provided by the sign of

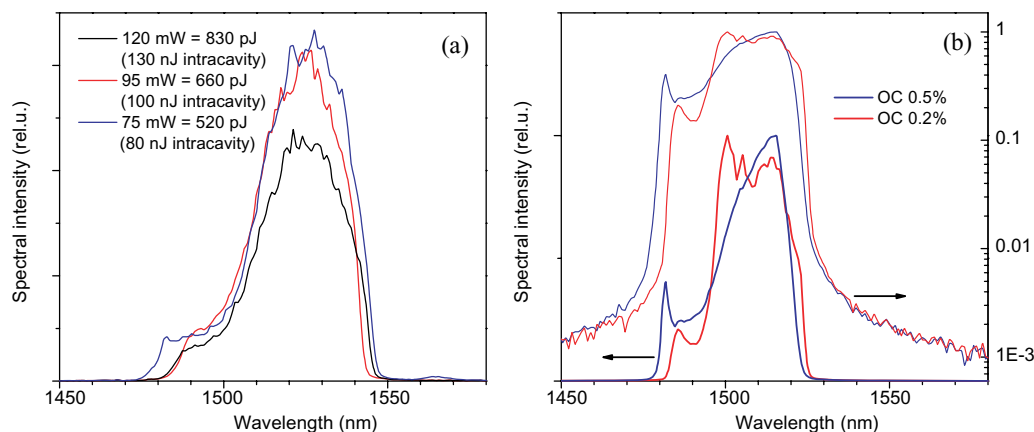


**Figure 3.** (a) Spectra of the Cr : YAG CPO at different values of intracavity pulse energy. (b) Spectra of the Cr : YAG CPO with different output couplers.

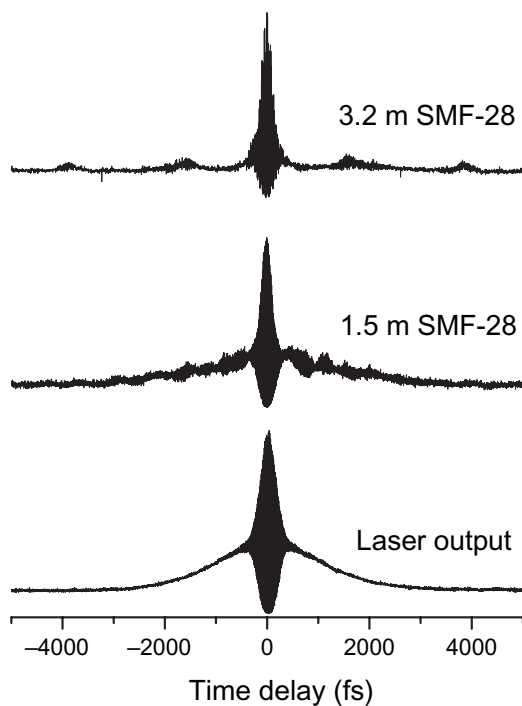


**Figure 4.** Extra-cavity pulse compression by a single-mode silica fiber.

the pulse chirp, which must be positive. In the  $1.5 \mu\text{m}$  wavelength range, compensation of the positive chirp can be made exceptionally easy by a piece of the silica fiber. Figure 4 shows some typical autocorrelation signals and estimated pulse durations after the propagation inside the standard telecom SMF-28 fiber. The maximum compression of the pulse duration from the initial 1.4 ps down to  $\approx 120$  fs occurs at a fiber length of about 3–3.5 m, and for the rest of the experiments a fiber piece of 3.2 m was used. The pulse compression is convincing proof of the positive chirp sign, and of the fact that the laser indeed operates in the positive dispersion regime.

The compressed pulses have sufficient peak power to produce supercontinuum generation in a 40 cm piece of a soft-glass PCF [20], as shown in figure 1.

To finish this section, we should also comment on the stability and reproducibility of the positive dispersion regime. Figure 3(a) demonstrates the spectra in one and the same setup assembled in Orsay (figure 1) at three different pulse energies. Figure 3(b) shows spectra obtained in a similar setup assembled in Vienna under Yb: fiber pumping. The dispersive mirrors and the crystal length were the same in both experiments, but the dichroic mirrors  $M_1$  and  $M_2$  (highly reflective around  $1.5 \mu\text{m}$  and transmissive around  $1 \mu\text{m}$ ) were different. It can be seen from these spectra that the CPO regime is quite reproducible and stable against fluctuations in intracavity pulse energy (figure 3(a)) and cavity losses (figure 3(b)) and, hence, against pump power fluctuations and small misalignments. This is important for possible applications [20]. At the same time, the output parameters are sensitive against the intracavity dispersion. This is evident from the fact that changing the dichroic mirrors can widen the spectra by  $\sim 25 \text{ nm}$  (compare figures 3(b) and (a); see also figure 8). The dichroic mirrors are positioned at large incidence angles of  $12\text{--}15^\circ$  and their dispersion is small, but not negligible. Given this sensitivity to dispersion variations, it is important to use the prismless techniques, which provide very reproducible and misalignment-insensitive intracavity dispersion.

### 3. Numerical modeling

#### 3.1. CPO modeling

Given the complex intracavity dispersion curve (figure 2(b)), we used the numerical simulation approach. Besides enabling us to cope with higher order dispersions, it permitted us to analyze the positive- and negative-dispersion regimes in a consistent way, to take into account the spectral distributions of gain and loss, and to provide results on the stability of operation regimes. The simulations were based on the generalized complex nonlinear cubic–quintic Ginzburg–Landau model [21], which has already proved to provide adequate description of the PDR [12, 13]. Within this model, the evolution of the slowly varying envelope  $A(z, t)$  of the intracavity field can be described in the following way:

$$\frac{\partial A}{\partial z} = \sigma(\omega_0)A + \alpha(\omega_0)\tau^2 \frac{\partial^2 A}{\partial t^2} - \rho(\omega - \omega'_0)A + i\beta(\omega - \omega_0)A + \{[\kappa - i\gamma]P - \kappa\zeta P^2\}A. \quad (1)$$

Here,  $z$  is the propagation distance normalized to the cavity length  $L_{\text{cav}}$  (i.e. the cavity round-trip number in the ring-cavity model) and  $t$  is the local time. The reference time frame moves with the pulse group-velocity defined at the reference frequency  $\omega_0$  corresponding to the gain maximum at  $\lambda_0 \approx 1.5 \mu\text{m}$ . The term  $\alpha(\omega_0)\tau^2 \partial^2 A / \partial t^2$  describes the action of the gain spectral profile in parabolic approximation. The parameter  $\alpha(\omega_0)$  is the saturated gain coefficient at  $\omega_0$ , and it is close to the net loss value at this frequency. The parameter  $\tau$  is the inverse gain bandwidth. The term  $\beta(\omega - \omega_0)A$  describes the net-GDD action in the Fourier domain. In particular cases, it can be expressed in the time domain through the series  $\beta(\omega - \omega_0)A = -\sum_{k=2}^N i^{k+1} \beta_k(\omega_0) \partial^k A / \partial t^k$ . The term  $\rho(\omega - \omega'_0)A$  describes the action of the net loss spectral profile in the Fourier domain. Frequency  $\omega'_0$  corresponds to the transmission minimum of the output coupler at  $\lambda'_0 = 1.53 \mu\text{m}$ .

The parameter  $\sigma(\omega_0)$  is the difference between the saturated gain  $\alpha(\omega_0)$  and the net loss at the reference frequency  $\omega_0$ . It is close to zero (rigorously zero in CW operation) and depends on the pulse energy due to gain saturation. Such a dependence can be

**Table 1.** Parameters of simulation.

Parameter	Value	Description
$\omega_0$	Corresponds to $\lambda_0 \approx 1.5 \mu\text{m}$	Gain central frequency
$\alpha(\omega_0)$	0.028	Saturated gain coefficient
$\tau$	9.5 fs	Inverse gain bandwidth
$\omega'_0$	Corresponds to $\lambda'_0 \approx 1.53 \mu\text{m}$	Loss central frequency
$\rho(\omega'_0)$	0.01	Minimal loss coefficient
$\gamma$	$1.8 \text{ MW}^{-1}$	Self-phase modulation parameter
$\kappa$	$0.05\gamma$	Self-amplitude modulation parameter
$\zeta$	$0.6\gamma$	Self-amplitude modulation saturation
$\delta$	-0.03	Stiffness coefficient
$E^*$	80 nJ	Intracavity pulse energy

linearized:  $\sigma(E) \approx \frac{d\sigma}{dE}|_{E=E^*}(E - E^*) = \delta(E/E^* - 1)$ , where  $E^*$  corresponds to the full energy stored inside an oscillator in the CW regime [13]. The parameter  $\delta \equiv \frac{d\sigma}{dE}|_{E=E^*}E^*$  defines the response of the active medium to the pulse energy  $E$  and is completely defined by the gain and loss coefficients (see [13] for a detailed discussion).

The parameter  $\gamma$  describes the self-phase modulation inside the active medium,  $\kappa$  is the self-amplitude modulation parameter and  $\zeta$  is the parameter defining saturation of the self-amplitude modulation with power [13]. The nonlinear parameters are related to the instantaneous power  $P \propto |A|^2$ , expressed in watts. Values of parameters used in simulations are presented in table 1.

Equation (1) is solved by the symmetrized split-step Fourier method in a 41 ps time window approximated by  $2^{15}$  points. The propagation step is  $10^{-3}$  of  $L_{\text{cav}}$ .

## 4. Results and discussion

### 4.1. PDR and spectrum asymmetry

As a starting point, we consider the simplest case of a Cr:YAG oscillator in the negative dispersion regime without the high-order dispersion terms in equation (1) (i.e.  $\beta = i\beta_2\partial^2 A/\partial t^2$ ), and with the minimum of the net losses shifted in  $\lambda'_0$  to match the experimental value. The spectral dependence of the net loss (transmission of the output coupler and the chirped mirrors, and SESAM absorption) is approximated by super-Gauss dependence  $\rho(\omega - \omega'_0) = \rho(\omega'_0) \exp[-100 \text{ fs}^6 \times (\omega - \omega'_0)^6]$ . In accord with the experiment, the simulations demonstrate that the operation in the NDR is unstable against the multipulsing within a wide region of negative dispersion  $\beta_2$ . The stable single-pulse regime appears only at very large amounts of negative GDD  $\beta_2 \approx -9900 \text{ fs}^2$ . The stable pulse is soliton-like and has a width of 230 fs. The comparatively narrow symmetric spectrum is centered at  $1.51 \mu\text{m}$  (gray curve in figure 5(a)). Such a pulse is chirp-free, linearly incompressible and does not reproduce the experimentally observed spectra (figure 3).

As already discussed, the observed spectra closely resemble those in the positive dispersion regime, and the next simulations concentrate on this regime. A striking feature of the observed spectra is their significant asymmetry (figure 3). Since the pulse in the PDR has a fairly broad

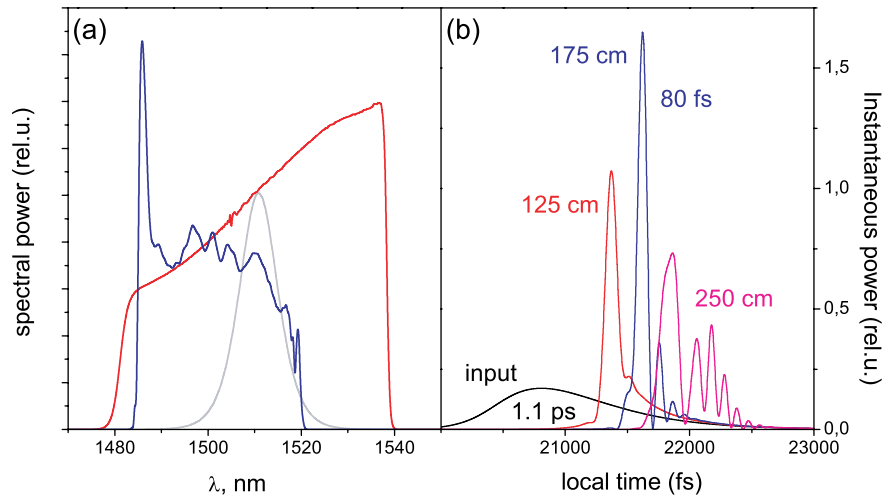


**Figure 5.** (a) Spectral profiles: GDD at  $\lambda'_0$  is  $200 \text{ fs}^2$  (red and blue curves) and  $-9900 \text{ fs}^2$  (gray curve). For the blue curve, the spectral losses are not taken into account. (b) Pulse profiles inside a fiber for the input pulse corresponding to the red solid curve in (a). Propagation lengths are indicated; minimum pulse width  $\approx 80 \text{ fs}$ .

spectrum, we expect that the high-order dispersions strongly affect the pulse characteristics [12]. Our simulation of the PDR therefore includes a significant amount of the third-order dispersion (TOD)  $\beta_3 = -10^3 \text{ fs}^3$  at  $\lambda'_0$ , which approximates the average TOD in figure 2. To single out the influence of the dispersion asymmetry we first ignore the spectral dependence of the losses (blue curve in figure 5(a)). We see that the spectrum indeed acquires asymmetry, but it has the opposite slope to that of the experimental spectra (figure 3). This agrees with the observation [12] that the TOD in the PDR results in the growth of those spectral components which are located within the region of the most positive GDD, i.e. at the short-wavelength side of the spectrum. However, this also means that the TOD alone cannot explain the observed spectral asymmetry.

In order to agree with the experiment, it is necessary to take into account the spectral dependence of losses in the cavity. In this case, the spectrum asymmetry is reversed (solid red curve in figure 5(a)), matching the observation. The asymmetry is somewhat less than in the experiment, because the model includes only the unsaturated loss profile. In mode-locked operation, the losses are modified due to the absorption saturation in the SESAM, which is not known.

The simulated down-compression of the picosecond chirped pulse outside of the cavity is illustrated by figure 5(b). Propagation inside a single-mode fused silica fiber would have compressed the pulse from  $1.1 \text{ ps}$  (black curve) down to  $80 \text{ fs}$  (blue line). Part of the energy is lost in the satellites formed due to non-uniform chirp of the input pulse [12, 15]. The calculation predicts a somewhat lower amount of chirp, a shorter output pulse duration and a shorter optimal fiber length for compensation than observed in the experiment. This can be connected with the presence of unknown high-order dispersion contributions to the intracavity dispersion (figure 2). Nevertheless, given the uncertainty in dispersion shape, the simulation matches the experiment very well and explains all observed features.

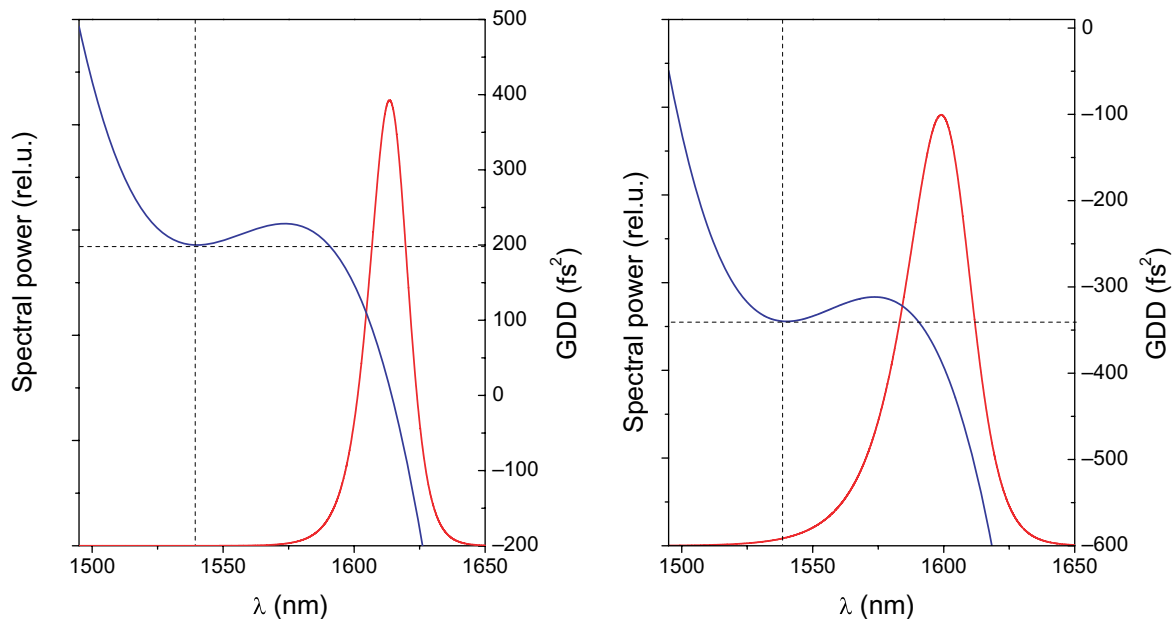


**Figure 6.** GDD spectral profiles (blue) and corresponding simulated pulse spectra (red) with no spectral dependence of the losses.

We thus conclude that the experimentally observed spectral asymmetry in the PDR is opposite to that caused by the TOD. Simulations demonstrate that such an asymmetry can be attributed to the action of spectrally dependent losses. However, in the general case, the oscillator spectrum and stability can be strongly affected by spectrally dependent net GDD, as well. Also, we need to consider the transitional regimes between the PDR and the NDR. These issues will be addressed in the next subsections.

#### 4.2. Effects of the GDD spectral shape: solitonic regime

Combination of different optical elements in the dispersion-compensated oscillator may result in a rather complex spectral profile of the GDD. This is especially true when multilayer chirped mirrors are used, which often introduce strong dispersion modulation. It is important therefore to explore the influence of the GDD modulation on the oscillator parameters.

Figure 6 shows the simulated spectra for the different GDD curves, which approximate the shape of the experimental net GDD and differ by only the value of  $\beta_2$  at  $\lambda = 1.54 \mu\text{m}$ , where the net GDD has a local minimum. Again, we assume no spectral dependence of the losses in this case. One can see that the asymmetric spectra are extremely red-shifted ( $> 70 \text{ nm}$ ) in comparison with the experimental ones. Such a red-shift has been analyzed in [8] for the much shorter  $\sim 20\text{--}30 \text{ fs}$  pulses, where high peak power caused additional nonlinear-optical effects, such as stimulated Raman scattering, to interfere.

The specific wavelength dependence of GDD causes two evident modifications of the solitonic regime: (i) there is the ‘mixed’ regime so that the spectrum is located within both negative and positive GDD ranges (figure 6, left graph) [14, 22]; (ii) NDR can be stable, when GDD is substantially closer to zero (figure 6, right graph) [8] in comparison with the case of the wavelength-independent  $\beta_2$  (in the latter case, the pulse is stabilized only at  $\beta_2 \approx -9900 \text{ fs}^2$ ;

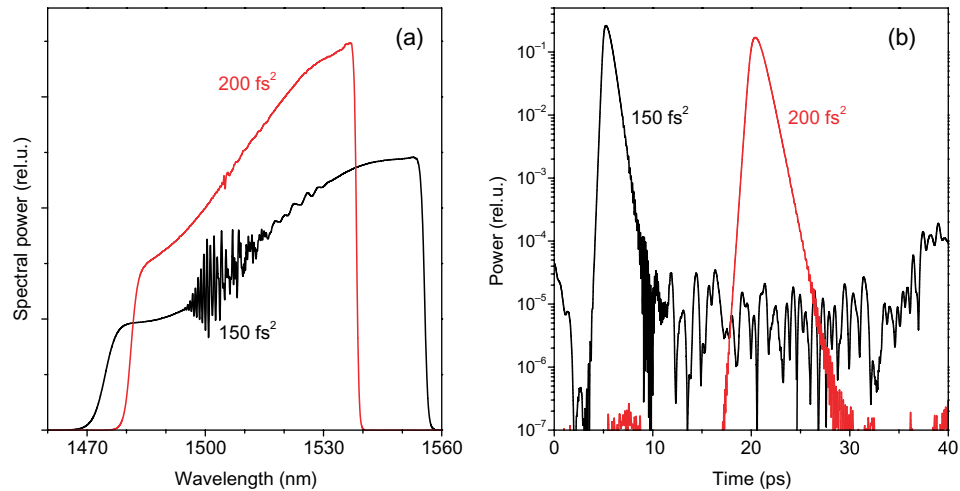


**Figure 7.** (a) Simulated spectra; (b) intensity profiles.  $\beta_2 = 200 \text{ fs}^2$  (red curves) and  $150 \text{ fs}^2$  (black curves), respectively. Other parameters correspond to figure 5, the case with spectrally dependent losses.

see section 4.1). When the GDD curve up-shifts (i.e.  $\beta_2$  at  $\lambda = 1.54 \text{ nm}$  increases), the spectrum shifts in the region of more negative GDD to provide the stability (i.e. the spectrum red-shifts; left graph of figure 6) [23]. When  $\beta_2$  at  $\lambda = 1.54 \text{ nm}$  exceeds  $200 \text{ fs}^2$ , the multipulsing appears.

The experiment as well as the simulations show that the solitonic regime in the vicinity of zero GDD has a low stability. For instance, the insertion of spectrally dependent losses in the simulations causes the multipulsing within the whole GDD range shown in figure 6.

#### 4.3. Scenario of the pulse destabilization

As pointed out earlier, the main scenario of the pulse destabilization in the NDR is multipulsing, when the GDD approaches zero or becomes positive within the pulse spectrum. However, such a scenario is not the only one for both PDR and NDR.

Firstly, let us consider PDR described in subsection 4.1. Figure 7 illustrates the effect of the  $\beta_2$  decrease. One can see (figure 7(a)) that the spectrum becomes broader when GDD at  $\lambda_0$  approaches zero. Additionally, the maximum shifts to longer wavelengths. Such a tendency is indeed visible in the experiment (figure 8, the transition from red to black curve corresponds to the approaching of the positive GDD to zero by  $40 \text{ fs}^2$  at  $1525 \text{ nm}$ ). Knowledge of these tendencies allows certain spectral shaping when required for applications. At low GDD values the pulse spectrum also develops ripples in the middle, where the net gain balances the net loss (figure 7(a), black curve). The multichannel InGaAs-array spectrometer cannot resolve the ripples, producing the residual modulation of the experimental spectra. In the time-domain, such ripples correspond to amplification of the CW background (figure 7(b), black curve). If there were no high-order dispersion or spectral filtering, the CW signal could not have coexisted with the chirped pulse and the latter would have become unstable [12, 13]. However, in our case such a ‘hybrid’ regime is stable (figure 7(b), black curve). A similar regime in the NDR has been demonstrated in [8].

Usually, the chirped mirrors, which are used for the GDD compensation, introduce the oscillating dependence of the GDD on wavelength. As it was pointed out in [8], this can modify

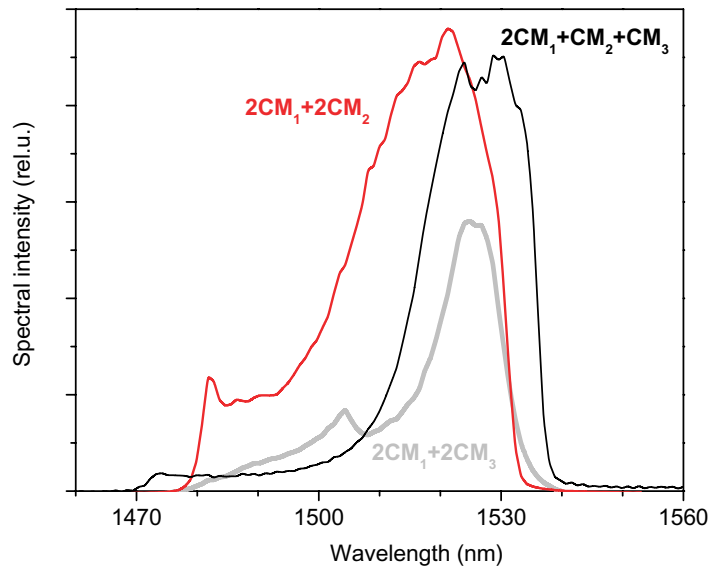


**Figure 8.** Experimental spectra of the CPO regime. The intracavity dispersion is changed by exchanging the mirrors. The actual mirror sets are used as labels. Red ( $2\text{CM}_1 + 2\text{CM}_2$ ) and black ( $2\text{CM}_1 + \text{CM}_2 + \text{CM}_3$ ) curves correspond to the CPO regime; the gray curve ( $2\text{CM}_1 + 2\text{CM}_3$ , not to the scale) represents a ‘chaotic’ mode-locking regime. Exchange of one  $\text{CM}_2$  mirror by a  $\text{CM}_3$  mirror reduces the round-trip GDD by about  $-40 \text{ fs}^2$  at  $1.53 \mu\text{m}$ .

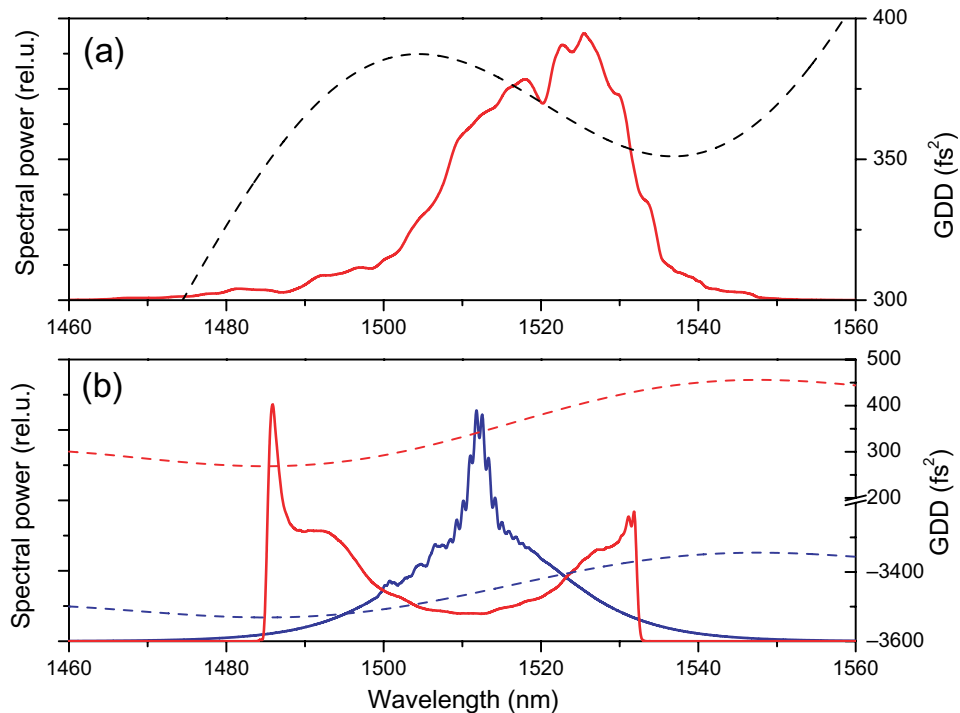
the stability conditions. Figure 9 shows the spectra for the cases when only the net GDD of the chirped mirrors and of the active medium is taken into account. The figures differ by the slope of GDD at  $\lambda = 1.54 \mu\text{m}$  (i.e. the local minimum of GDD at this wavelength in figure 9(a) and the local maximum in figure 9(b)), as well as by the  $\beta_2(\lambda = 1.54 \mu\text{m})$  value.

Figure 9(a) shows the ‘chaotic’ PDR [19], which appears when the dispersion curve further approaches zero (down-shifts). Such a regime is also experimentally observable (gray curve in figure 8). In calculations, it exists only if there is a wavelength dependence of the GDD. In this case, the spectrum shifts to the local GDD minimum. It was shown previously [19] that the PDR stability is improved in the vicinity of the local minimum of the GDD (positive fourth-order dispersion).

Figure 9(b) shows the spectra corresponding to the upper stability border of NDR (blue curves) and the lower stability border of PDR (red curves) for a given GDD shape. The shown NDR (blue curve) is the ‘chaotic’ mode-locking when the pulse is strongly perturbed and its peak power chaotically oscillates. Further GDD increase (i.e. the up-shift of the GDD curve) results in multipulsing. The multipulsing changes to the ‘chaotic’ mode-locking in the PDR. When the GDD reaches some positive threshold value, the stable chirped pulse appears (red curve).

## 5. Conclusion

We have observed and described the first chirped-pulsed operation of a Cr:YAG femtosecond oscillator in a positive dispersion regime. The oscillator emits strongly chirped 1.4 ps pulses



**Figure 9.** Simulated spectra (solid curves), with different net GDD values (dashed curves).  $\lambda_0 = 1.54 \mu\text{m}$ ; other parameters correspond to figure 5, the case without spectrally dependent losses.

with a typical side-cut spectrum of  $\sim 60$  nm width, which can be conveniently compressed in a piece of silica fiber down to  $\sim 100$  fs duration. The chirped-pulse regime of operation is stable and reproducible, allowing us to use the oscillator for applications, as reported in [20], by obtaining high-resolution molecular spectra through supercontinuum generation in a nonlinear photonic-crystal fiber.

Simulations based on the generalized complex nonlinear cubic–quintic Ginzburg–Landau model demonstrate that the experimentally observed spectral asymmetry is opposite to that caused by only a third-order dispersion and results from the spectral dependence of the net loss. It is shown that there exist two scenarios of the chirped-pulse destabilization: CW amplification and chaotic-mode-locking.

When operated in the conventional negative dispersion regime, the same oscillator exhibits a strong tendency to harmonic mode-locking (i.e. multipulsing), making further spectrum broadening through supercontinuum generation impossible. The GDD value providing the multipulsing suppression depends on the GDD shape, so that the soliton-like regime can exist even if the part of the spectrum lies within the positive dispersion range. However, in all considered cases, the positive- and negative-dispersion single-pulse regimes are disjointed by the GDD ranges with chaotic and harmonic mode-locking.

The transition from the conventional soliton regime to chirped pulse allowed the pulse energy to be increased by a factor of 5 from 0.2 to 1 nJ for a given oscillator configuration, which was critical to achieve the supercontinuum in the nonlinear fiber. The demonstration of the well-controlled chirped pulse regime opens the way to further pulse-energy increase in Cr: YAG oscillators by cavity-extension techniques.

## Acknowledgments

O Okhotnikov (Tampere University of Technology) is gratefully acknowledged for providing the samples of nonlinear fiber. This work was performed within the framework of the Programme Pluri-Formation de l'Université Paris-Sud 'Détection de traces de gaz' 2006–2009 and the Austrian Fonds zur Förderung der wissenschaftlichen Forschung projects P17973 and P20293, and supported by the Austrian–French program *Amadée* and the French–Norwegian program *Aurora*.

## References

- [1] Sorokin E, Kalashnikov V L, Naumov S, Teipel J, Warken F, Giessen H and Sorokina I T 2003 *Appl. Phys. B* **77** 197
- [2] Kalashnikov V L, Sorokin E, Naumov S, Sorokina I T, Ravi Kanth Kumar V V and George K 2004 *Appl. Phys. B* **79** 591
- [3] Mandon J, Guelachvili G., Picqué N, Druon F and Georges P 2007 *Opt. Lett.* **32** 1677
- [4] Sorokin E, Naumov S and Sorokina I T 2005 *IEEE J. Sel. Top. Quantum Electron.* **11** 690
- [5] Naumov S, Sorokin E, Kalashnikov V L, Tempea G and Sorokina I T 2003 *Appl. Phys. B* **76** 11
- [6] Kalashnikov V L, Sorokin E and Sorokina I T 2003 *IEEE J. Quantum Electron.* **39** 323
- [7] Sorokin E, Kalashnikov V L, Naumov S, Teipel J, Meiser D, Giessen H and Sorokina I T 2003 *Appl. Phys. B* **77** 197
- [8] Kalashnikov V L, Sorokin E, Naumov S and Sorokina I T 2003 *J. Opt. Soc. Am.* **20** 2084
- [9] Leburn C G, Lagatsky A A, Brown C T A and Sibbett W 2004 *Electron. Lett.* **40** 805
- [10] Proctor B, Westwig E and Wise F 1993 *Opt. Lett.* **18** 1654
- [11] Haus H A, Fujimoto J G and Ippen E P 1991 *J. Opt. Soc. Am.* **B 8** 2068
- [12] Kalashnikov V L, Podivilov E, Chernykh A, Naumov S, Fernandez A, Graf R and Apolonski A 2005 *New J. Phys.* **7** 217
- [13] Kalashnikov V L, Podivilov E, Chernykh A and Apolonski A 2006 *Appl. Phys. B* **83** 503
- [14] Dudley J M, Boussen S M, Cameron D M J and Harvey J D 1999 *Appl. Opt.* **38** 3308
- [15] Naumov S, Fernandez A, Graf R, Dombi P, Krausz F and Apolonski A 2005 *New J. Phys.* **7** 216
- [16] Fernández A, Verhoef A, Pervak V, Lermann G, Krausz F and Apolonski A 2007 *Appl. Phys. B* **87** 395
- [17] Chong A, Renninger W H and Wise F W 2008 *J. Opt. Soc. Am.* **B 25** 140
- [18] Naumov S, Sorokin E and Sorokina I T 2003 *OSA Trends in Optics and Photonics* vol 83 *Advanced Solid-State Photonics* (Washington, DC: Optical Society of America) p 163
- [19] Kalashnikov V L, Fernández A and Apolonski A 2008 *Opt. Express* **16** 4206
- [20] Mandon J, Sorokin E, Sorokina I T, Guelachvili G and Picqué N 2008 *Opt. Lett.* **33** 285
- [21] Akhmediev N N and Ankiewicz A 1997 *Solitons: Nonlinear Pulses and Beams* (London: Chapman and Hall)
- [22] Rundquist A, Durfee C, Chang Z, Taft G, Zeek E, Backus S, Murnane M M, Kapteyn H C, Christov I and Stoev V 1997 *Appl. Phys. B* **65** 161
- [23] Jung I D, Kärtner F X, Henkmann J, Zhang G and Keller U 1997 *Appl. Phys. B* **65** 307